Nano-Hexapod - Test Bench

Dehaeze Thomas

October 27, 2024

Contents

In the previous section, all the struts were mounted and individually characterized. Now the nano-hexapod is assembled using a mounting procedure described in Section 1.

In order to identify the dynamics of the nano-hexapod, a special suspended table is developed which consists of a stiff "optical breadboard" suspended on top of four soft springs. The Nano-Hexapod is then fixed on top of the suspended table, such that its dynamics is not affected by complex dynamics except from the suspension modes of the table that can be well characterized and modelled (Section 2).

The obtained nano-hexapod dynamics is analyzed in Section 3, and compared with the Simscape model in Section 4.

1 Nano-Hexapod Assembly Procedure

The assembly of the nano-hexapod is quite critical to both avoid additional stress in the flexible joints (that would result in a loss of stroke) and for the precise determination of the Jacobian matrix. The goal is to fix the six struts to the two nano-hexapod plates (shown in Figure 1.1a) while the two plates are parallel, aligned vertically, and such that all the flexible joints do not experience any stress. Do to so, a precisely machined mounting tool (Figure 1.1b) is used to position the two nano-hexapod plates during the assembly procedure.
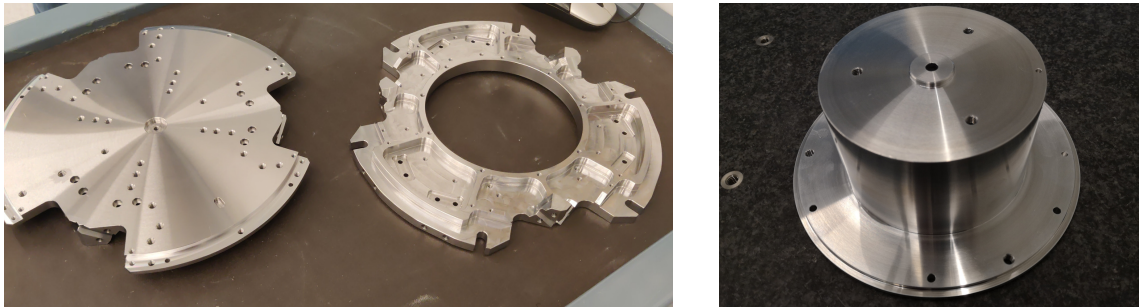
(a) Received top and bottom plates

(b) Mounting tool

Figure 1.1: Received Nano-Hexapod plates (a) and mounting tool used to position the two plates during assembly (b)

The mechanical tolerances of the received plates are checked using a FARO arm[1] (Figure 1.2a) and are found to comply with the requirements[2]. The same is done for the mounting tool[3] The two plates are then fixed to the mounting tool as shown in Figure 1.2b. The main goal of this "mounting tool" is to position the flexible joint interfaces (the "V" shapes) of both plates such that a cylinder can rest on the 4 flat interfaces at the same time.

The quality of the positioning can be estimated by measuring the "straightness" of the top and bottom "V" interfaces. This corresponds to the diameter of the smallest cylinder that contains all points of the measured axis. This is again done using the FARO arm, and the results for all the six struts are summarized in Table 1.1. The straightness is found to be better than $15\,\mu m$ for all the struts[4], which is sufficiently good to not induce significant stress of the flexible joint during the assembly.

The encoder rulers and heads are then fixed to the top and bottom plates respectively (Figure 1.3). The encoder heads are then aligned to maximize the received contrast.

The six struts are then fixed to the bottom and top plates one by one. First the top flexible joint is

---

[1]Faro Arm Platinum 4ft, specified accuracy of $\pm 13\mu m$

[2]Location of all the interface surfaces with the flexible joints are checked. The fits (182H7 and 24H8) with the interface element are checked.

[3]The height dimension is better than $40\,\mu m$. The diameter fit of 182g6 and 24g6 with the two plates is verified.

[4]As the accuracy of the FARO arm is $\pm 13\,\mu m$, the true straightness is probably better than the values indicated. The limitation of the instrument is here reached.
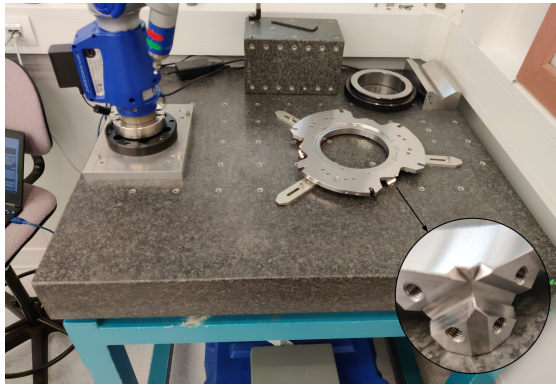
(a) Dimensional check of the bottom plate
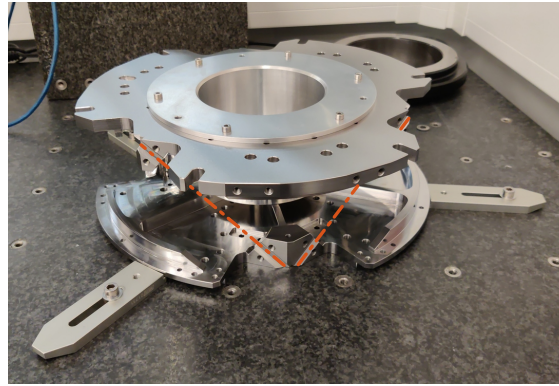
(b) Wanted coaxiality between interfaces

Figure 1.2: A Faro arm is used to dimensionally check the received parts (a) and after mounting the two plates with the mounting part (b)

Strut	Meas 1	Meas 2
1	$7\,\mu m$	$3\,\mu m$
2	$11\,\mu m$	$11\,\mu m$
3	$15\,\mu m$	$14\,\mu m$
4	$6\,\mu m$	$6\,\mu m$
5	$7\,\mu m$	$5\,\mu m$
6	$6\,\mu m$	$7\,\mu m$

Table 1.1: Measured straightness between the two "V" for the six struts. These measurements are performed two times for each strut.

(a) Encoder rulers
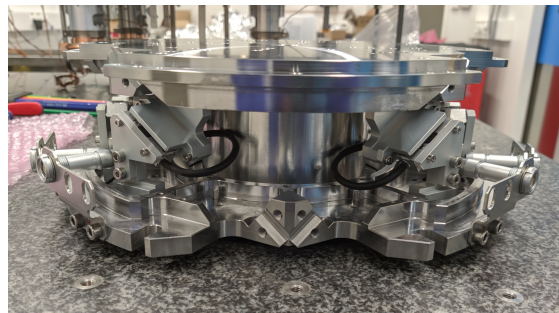
(b) Encoder heads

Figure 1.3: Mounting of the encoders to the Nano-hexapod. The rulers are fixed to the top plate (a) while the encoders heads are fixed to the botom plate (b)

fixed such that its flat reference surface is in contact with the top plate. This is to precisely known the position of the flexible joint with respect to the top plate. Then the bottom flexible joint is fixed. After all six struts are mounted, the mounting tool (Figure 1.1b) can be disassembled, and the fully mounted nano-hexapod as shown in Figure 1.4 is obtained.
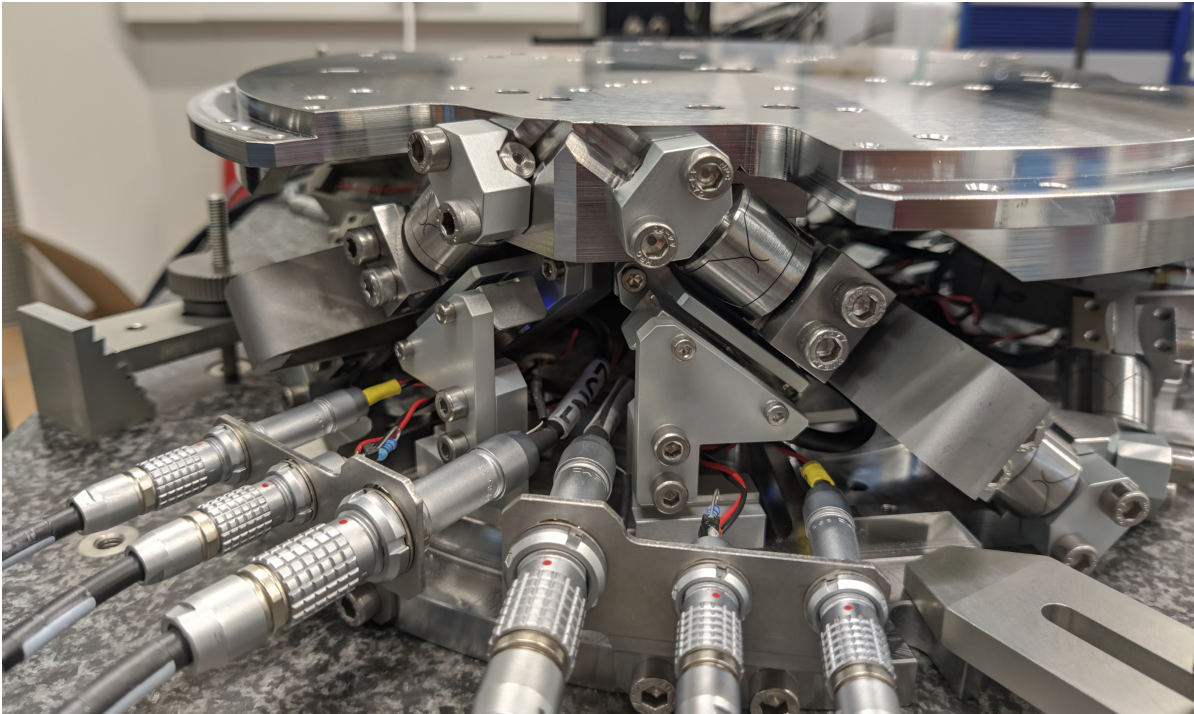
Figure 1.4: Mounted Nano-Hexapod

2 Suspended Table

2.1 Introduction

When a dynamical system is fixed to a support (such as a granite or an optical table), its dynamics will couple to the support dynamics. This may results in additional modes appearing in the system dynamics, which are difficult to predict and model. Two prevent this issue, strategy adopted here is to mount the nano-hexapod on top a suspended table with low frequency suspension modes.

In such a case, the modes of the suspended table are chosen to be at much lower frequency than those of the nano-hexapod such that they are well decoupled. An other key advantage is that the suspension modes of the suspended table can be easily modelled using Simscape. Therefore, the measured dynamics of the nano-hexapod on top of the suspended table can be compared to a simscape model representing the same experimental conditions. The model of the Nano-Hexapod can thus be precisely tuned to match the measured dynamics.

The developed suspended table is presented in Section 2.2. The modal analysis of the table is done in 2.3. Finally, the Simscape model representing the suspended table is tuned to match the measured modes (Section 2.4).

2.2 Experimental Setup

The design of the suspended table is quite straightforward. First, an optical table with high frequency flexible mode was selected[1]. Then, four springs[2] were selected with low enough spring rate such that the suspension modes are below 10Hz. Finally, some interface elements were designed, and mechanical lateral mechanical stops were added (Figure 2.1).
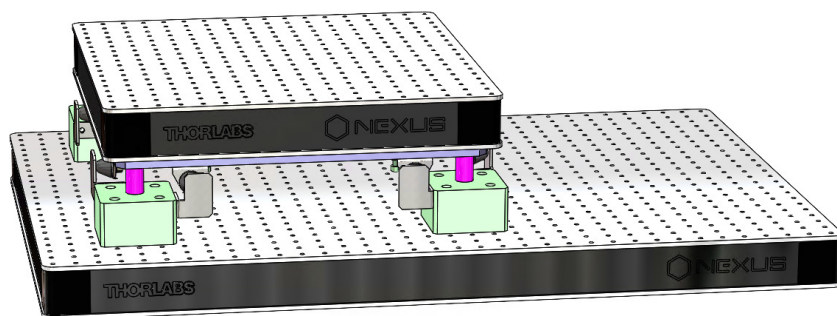
**Figure 2.1:** CAD View of the vibration table. Purple cylinders are representing the soft springs.

---

[1]The 450 mm x 450 mm x 60 mm Nexus B4545A from Thorlabs.
[2]"SZ8005 20 x 044" from Steinel. The spring rate is specified at $17.8 \, N/mm$

2.3 Modal analysis of the suspended table

In order to perform a modal analysis of the suspended table, a total of 15 3-axis accelerometers[3] were fixed to the breadboard. Using an instrumented hammer, the first 9 modes could be identified and are summarized in Table 2.1. The first 6 modes are suspension modes (i.e. rigid body mode of the breadboard) and are located below 10Hz. The next modes are flexible modes of the breadboard as shown in Figure 2.3, and located above 700Hz.
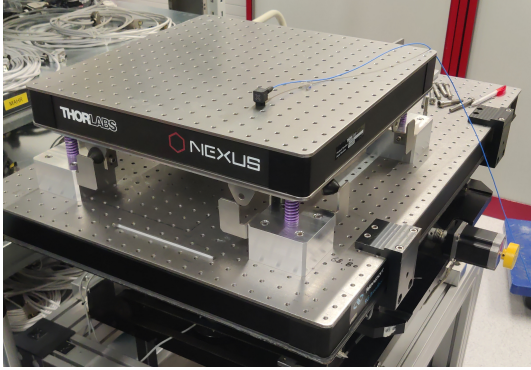
Figure 2.2: Mounted suspended table. Only 1 or the 15 accelerometer is mounted on top

Modes	Frequency	Description
1,2	1.3 Hz	X-Y translations
3	2.0 Hz	Z rotation
4	6.9 Hz	Z translation
5,6	9.5 Hz	X-Y rotations
7	701 Hz	"Membrane" Mode
8	989 Hz	Complex mode
9	1025 Hz	Complex mode

Table 2.1: Obtained modes of the suspended table

(a) Flexible mode at 701Hz

(b) Flexible mode at 989Hz


(c) Flexible mode at 1025Hz
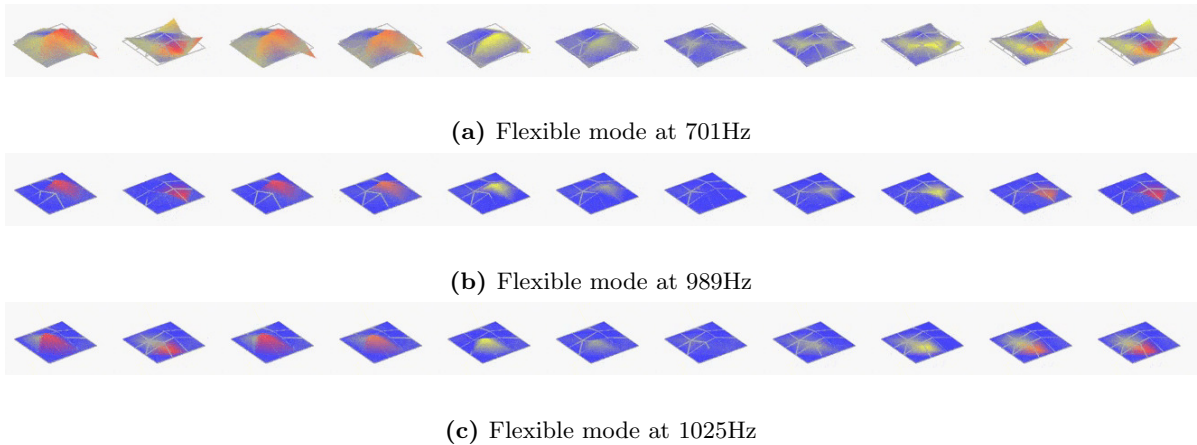
Figure 2.3: Three identified flexible modes of the suspended table

2.4 Simscape Model of the suspended table

The Simscape model of the suspended table simply consists of two solid bodies connected by 4 springs. The 4 springs are here modelled with "bushing joints" that have stiffness and damping properties in x, y and z directions. The 3D representation of the model is displayed in Figure 2.4 where the 4 "bushing joints" are represented by the blue cylinders.

---

[3]PCB 356B18. Sensitivity is $1\,V/g$, measurement range is $\pm 5\,g$ and bandwidth is 0.5 to 5 kHz.
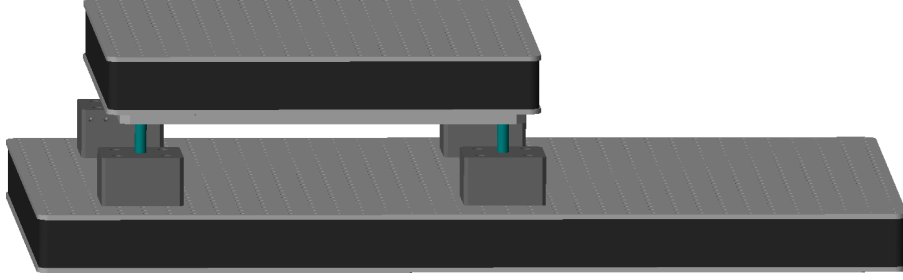
**Figure 2.4:** 3D representation of the simscape model

The model order is 12, and it represents the 6 suspension modes. The inertia properties of the parts are set from the geometry and material densities. The stiffness of the springs was initially set from the datasheet nominal value of $17.8\,N/mm$ and then reduced down to $14\,N/mm$ to better match the measured suspension modes. The stiffness of the springs in the horizontal plane is set at $0.5\,N/mm$. The obtained suspension modes of the simscape model are compared with the measured ones in Table 2.2.

Directions	D_x, D_y	R_z	D_z	R_x, R_y
Experimental	1.3 Hz	2.0 Hz	6.9 Hz	9.5 Hz
Simscape	1.3 Hz	1.8 Hz	6.8 Hz	9.5 Hz

Table 2.2: Comparison of the identified suspension modes with the Simscape model and measured experimentally

3 Nano-Hexapod Dynamics

In Figure 3.1 is shown a block diagram of the experimental setup. When possible, the notations are consistent with this diagram and summarized in Table 3.1.

figs/test_nhexa_nano_hexapod_signals.pdf
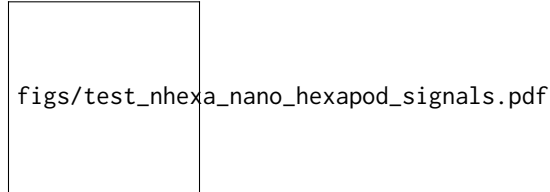
Figure 3.1: Block diagram of the system with named signals

|	Unit	Matlab	Vector	Elements
Control Input (wanted DAC voltage)	[V]	u	$\boldsymbol{u}$	u_i
DAC Output Voltage	[V]	u	$\tilde{\boldsymbol{u}}$	$\tilde{u}_i$
PD200 Output Voltage	[V]	ua	$\boldsymbol{u}_a$	$u_{a,i}$
Actuator applied force	[N]	tau	$\boldsymbol{\tau}$	τ_i
Strut motion	[m]	dL	$d\boldsymbol{\mathcal{L}}$	$d\mathcal{L}_i$
Encoder measured displacement	[m]	dLm	$d\boldsymbol{\mathcal{L}}_m$	$d\mathcal{L}_{m,i}$
Force Sensor strain	[m]	epsilon	$\boldsymbol{\epsilon}$	ϵ_i
Force Sensor Generated Voltage	[V]	taum	$\tilde{\boldsymbol{\tau}}_m$	$\tilde{\tau}_{m,i}$
Measured Generated Voltage	[V]	taum	$\boldsymbol{\tau}_m$	$\tau_{m,i}$
Motion of the top platform	[m,rad]	dX	$d\boldsymbol{\mathcal{X}}$	$d\mathcal{X}_i$
Metrology measured displacement	[m,rad]	dXm	$d\boldsymbol{\mathcal{X}}_m$	$d\mathcal{X}_{m,i}$

Table 3.1: List of signals

It is structured as follow:

- Section 3.1: The dynamics of the nano-hexapod is identified.

- Section 4.1: The identified dynamics is compared with the Simscape model.

3.1 Identification of the dynamics

In this section, the dynamics of the nano-hexapod with the encoders fixed to the plates is identified.

First, the measurement data are loaded in Section 3.1.1, then the transfer function matrix from the actuators to the encoders are estimated in Section 3.1.2. Finally, the transfer function matrix from the actuators to the force sensors is estimated in Section 3.1.3.
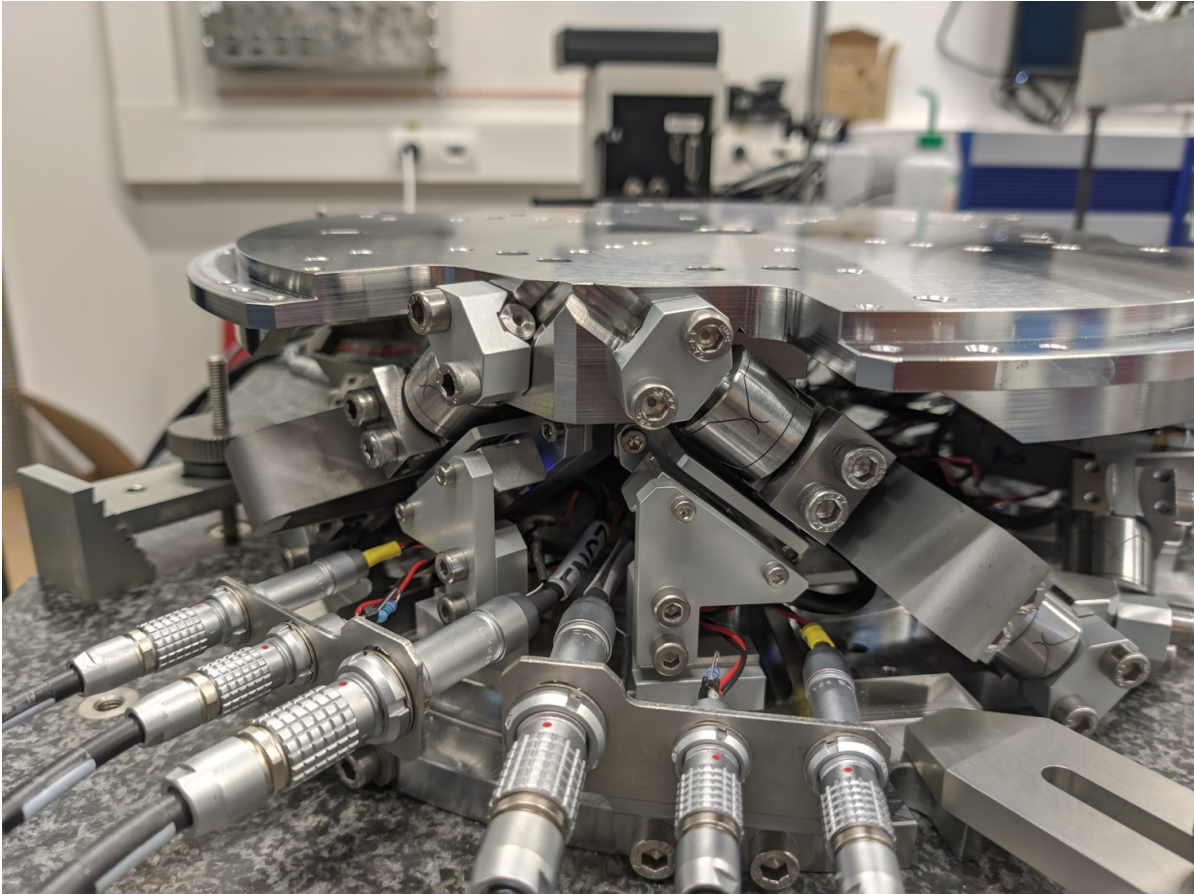
**Figure 3.2:** Nano-Hexapod with encoders fixed to the struts

3.1.1 Data Loading and Spectral Analysis Setup

The actuators are excited one by one using a low pass filtered white noise. For each excitation, the 6 force sensors and 6 encoders are measured and saved.

3.1.2 Transfer function from Actuator to Encoder

The 6x6 transfer function matrix from the excitation voltage u and the displacement $d\mathcal{L}_m$ as measured by the encoders is estimated.

The diagonal and off-diagonal terms of this transfer function matrix are shown in Figure 3.3.
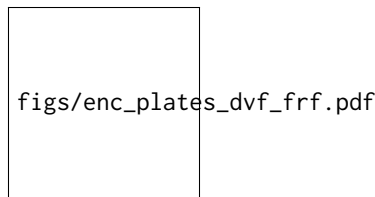
Figure 3.3: Measured FRF for the transfer function from u to $d\mathcal{L}_m$

> **Important**
>
> From Figure 3.3, we can draw few conclusions on the transfer functions from u to $d\mathcal{L}_m$ when the encoders are fixed to the plates:
>
> - the decoupling is rather good at low frequency (below the first suspension mode). The low frequency gain is constant for the off diagonal terms, whereas when the encoders where fixed to the struts, the low frequency gain of the off-diagonal terms were going to zero (Figure **??**).
>
> - the flexible modes of the struts at 226Hz and 337Hz are indeed shown in the transfer functions, but their amplitudes are rather low.
>
> - the diagonal terms have alternating poles and zeros up to at least 600Hz: the flexible modes of the struts are not affecting the alternating pole/zero pattern. This what not the case when the encoders were fixed to the struts (Figure **??**).

3.1.3 Transfer function from Actuator to Force Sensor

Then the 6x6 transfer function matrix from the excitation voltage u and the voltage τ_m generated by the Force senors is estimated. The bode plot of the diagonal and off-diagonal terms are shown in Figure 3.4.

> **Important**
>
> It is shown in Figure 4.2 that:
> - The IFF plant has alternating poles and zeros

Figure 3.4: Measured FRF for the IFF plant

- The first flexible mode of the struts as 235Hz is appearing, and therefore is should be possible to add some damping to this mode using IFF

- The decoupling is quite good at low frequency (below the first model) as well as high frequency (above the last suspension mode, except near the flexible modes of the top plate)

3.1.4 Save Identified Plants

The identified dynamics is saved for further use.

3.2 Effect of Payload mass on the Dynamics

In this section, the encoders are fixed to the plates, and we identify the dynamics for several payloads. The added payload are half cylinders, and three layers can be added for a total of around 40kg (Figure 3.5).

First the dynamics from $\boldsymbol{u}$ to $d\mathcal{L}_m$ and $\boldsymbol{\tau}_m$ is identified. Then, the Integral Force Feedback controller is developed and applied as shown in Figure 3.6. Finally, the dynamics from $\boldsymbol{u}'$ to $d\mathcal{L}_m$ is identified and the added damping can be estimated.

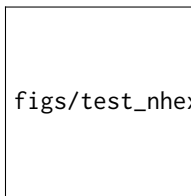### 3.2.1 Measured Frequency Response Functions

The following data are loaded:

- `Va` : the excitation voltage (corresponding to u_i)

- `Vs` : the generated voltage by the 6 force sensors (corresponding to $\boldsymbol{\tau}_m$)

- `de` : the measured motion by the 6 encoders (corresponding to $d\boldsymbol{\mathcal{L}}_m$)

The window `win` and the frequency vector `f` are defined. Finally the 6×6 transfer function matrices from $\boldsymbol{u}$ to $d\mathcal{L}_m$ and from $\boldsymbol{u}$ to $\boldsymbol{\tau}_m$ are identified: The identified dynamics are then saved for further use.
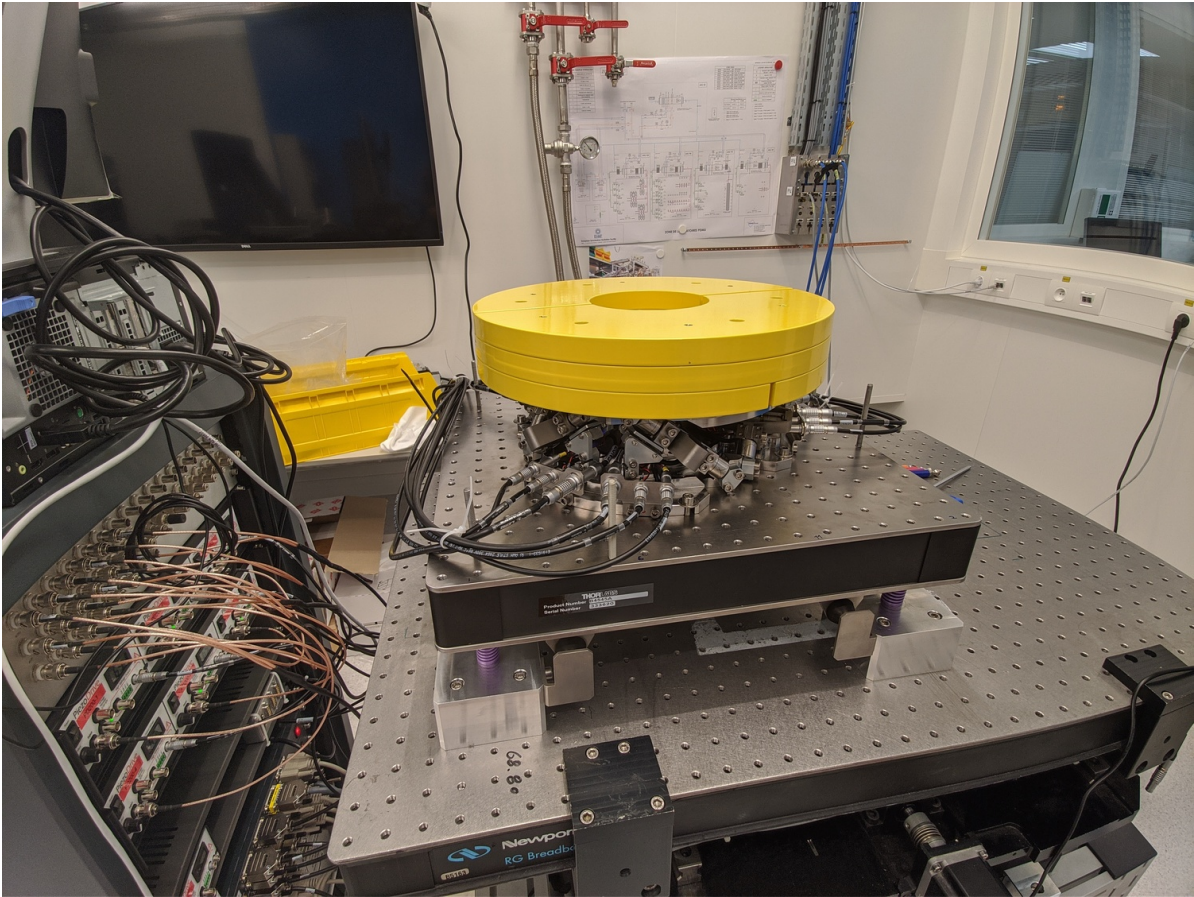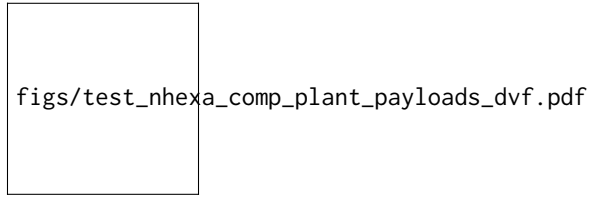
Figure 3.5: Picture of the nano-hexapod with added mass

Figure 3.6: Block Diagram of the experimental setup and model

3.2.2 Transfer function from Actuators to Encoders

The transfer functions from $\boldsymbol{u}$ to $d\boldsymbol{\mathcal{L}}_m$ are shown in Figure 3.7.

Figure 3.7: Measured Frequency Response Functions from u_i to $d\mathcal{L}_{m,i}$ for all 4 payload conditions. Diagonal terms are solid lines, and shaded lines are off-diagonal terms.
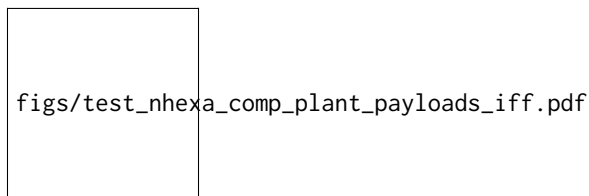
> **Important**
>
> From Figure 3.7, we can observe few things:
>
> - The obtained dynamics is changing a lot between the case without mass and when there is at least one added mass.
>
> - Between 1, 2 and 3 added masses, the dynamics is not much different, and it would be easier to design a controller only for these cases.
>
> - The flexible modes of the top plate is first decreased a lot when the first mass is added (from 700Hz to 400Hz). This is due to the fact that the added mass is composed of two half cylinders which are not fixed together. Therefore is adds a lot of mass to the top plate without adding a lot of rigidity in one direction. When more than 1 mass layer is added, the half cylinders are added with some angles such that rigidity are added in all directions (see Figure 3.5). In that case, the frequency of these flexible modes are increased. In practice, the payload should be one solid body, and we should not see a massive decrease of the frequency of this flexible mode.
>
> - Flexible modes of the top plate are becoming less problematic as masses are added.
>
> - First flexible mode of the strut at 230Hz is not much decreased when mass is added. However, its apparent amplitude is much decreased.

3.2.3 Transfer function from Actuators to Force Sensors

The transfer functions from $\boldsymbol{u}$ to $\boldsymbol{\tau}_m$ are shown in Figure 3.8.
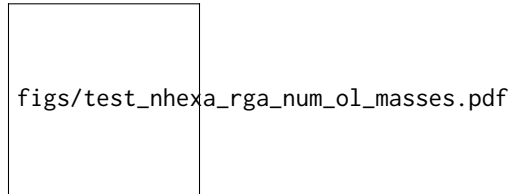

Figure 3.8: Measured Frequency Response Functions from u_i to $\tau_{m,i}$ for all 4 payload conditions. Diagonal terms are solid lines, and shaded lines are off-diagonal terms.

3.2.4 Coupling of the transfer function from Actuator to Encoders

The RGA-number, which is a measure of the interaction in the system, is computed for the transfer function matrix from $\boldsymbol{u}$ to $d\boldsymbol{\mathcal{L}}_m$ for all the payloads. The obtained numbers are compared in Figure 3.9.

figs/test_nhexa_rga_num_ol_masses.pdf

Figure 3.9: RGA-number for the open-loop transfer function from $\boldsymbol{u}$ to $d\boldsymbol{\mathcal{L}}_m$

3.3 Conclusion

4 Comparison with the Nano-Hexapod model?

4.1 Comparison with the Simscape Model

In this section, the measured dynamics done in Section 3.1 is compared with the dynamics estimated from the Simscape model.

A configuration is added to be able to put the nano-hexapod on top of the vibration table as shown in Figure 4.1.
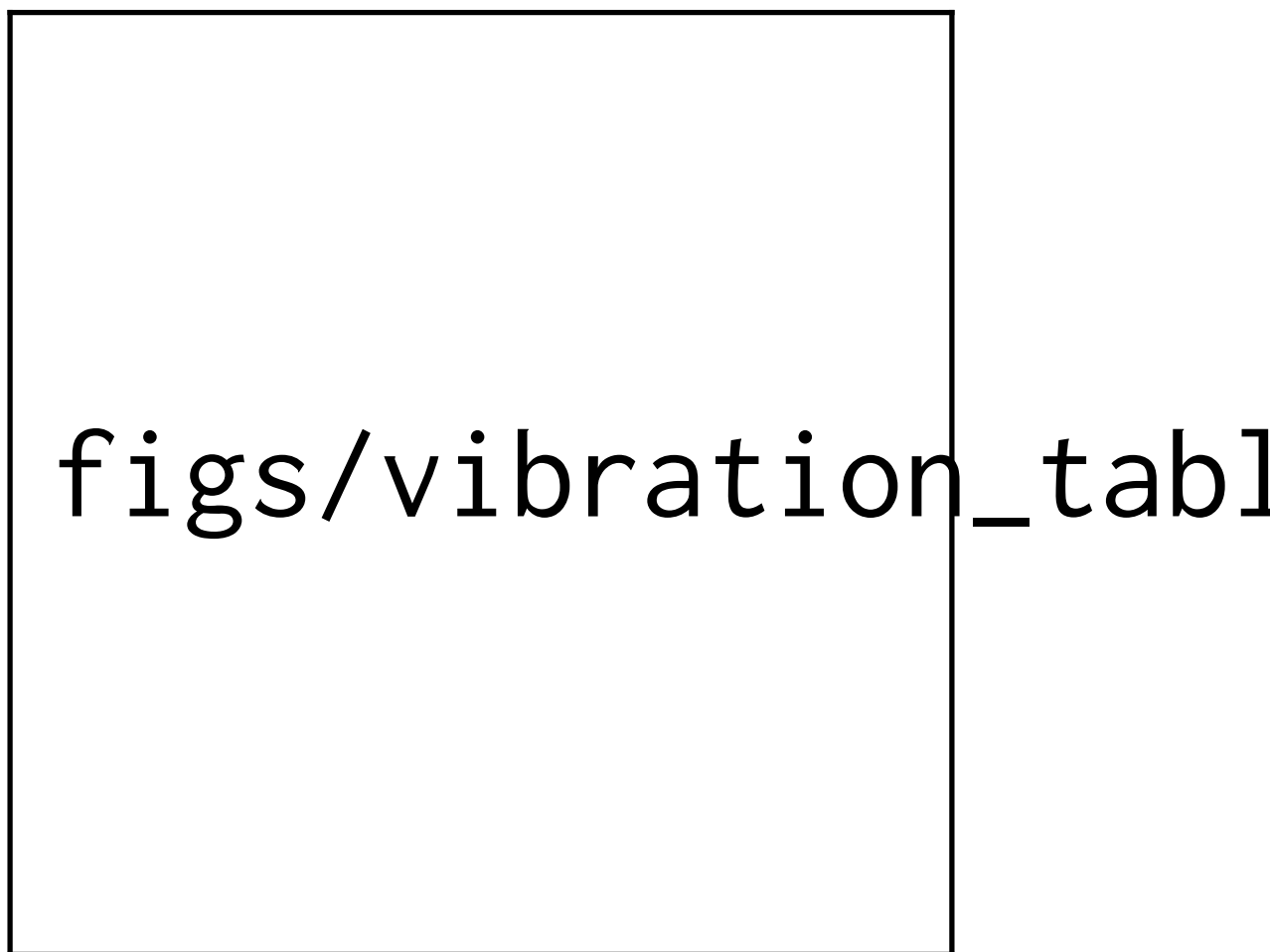

Figure 4.1: 3D representation of the simscape model with the nano-hexapod

4.1.1 Identification with the Simscape Model

The nano-hexapod is initialized with the APA taken as 2dof models. Now, the dynamics from the DAC voltage u to the encoders $d\mathcal{L}_m$ is estimated using the Simscape model. Then the transfer function from u to τ_m is identified using the Simscape model. The identified dynamics is saved for further use.
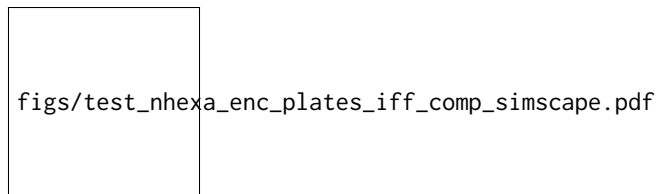
4.1.2 Dynamics from Actuator to Force Sensors

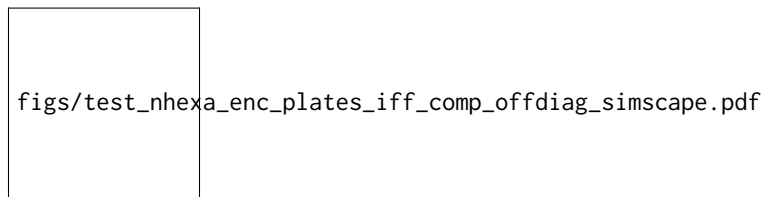The identified dynamics is compared with the measured FRF:

- Figure 4.2: the individual transfer function from u_1 (the DAC voltage for the first actuator) to the force sensors of all 6 struts are compared

- Figure 4.3: all the diagonal elements are compared

- Figure 4.4: all the off-diagonal elements are compared

figs/test_nhexa_enc_plates_iff_comp_simscape_all.pdf
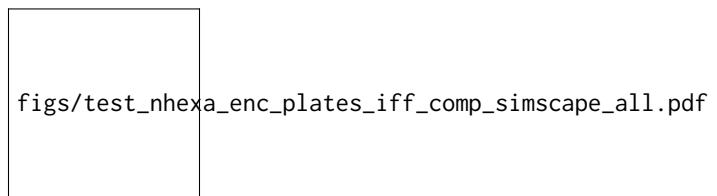
Figure 4.2: IFF Plant for the first actuator input and all the force senosrs

figs/test_nhexa_enc_plates_iff_comp_simscape.pdf

Figure 4.3: Diagonal elements of the IFF Plant

figs/test_nhexa_enc_plates_iff_comp_offdiag_simscape.pdf

Figure 4.4: Off diagonal elements of the IFF Plant

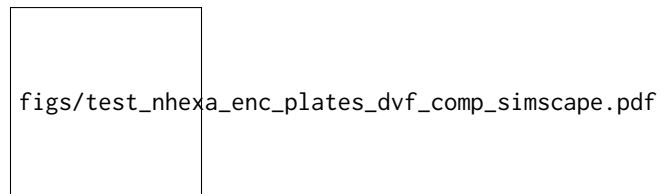### 4.1.3 Dynamics from Actuator to Encoder

The identified dynamics is compared with the measured FRF:

- Figure 4.5: the individual transfer function from u_3 (the DAC voltage for the actuator number 3) to the six encoders
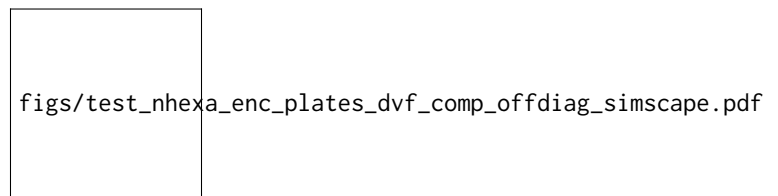
- Figure 4.6: all the diagonal elements are compared

- Figure 4.7: all the off-diagonal elements are compared

figs/test_nhexa_enc_plates_dvf_comp_simscape_all.pdf

Figure 4.5: DVF Plant for the first actuator input and all the encoders

figs/test_nhexa_enc_plates_dvf_comp_simscape.pdf

Figure 4.6: Diagonal elements of the DVF Plant

figs/test_nhexa_enc_plates_dvf_comp_offdiag_simscape.pdf

Figure 4.7: Off diagonal elements of the DVF Plant

4.1.4 Conclusion

> **Important**
>
> The Simscape model is quite accurate for the transfer function matrices from $\boldsymbol{u}$ to $\boldsymbol{\tau}_m$ and from $\boldsymbol{u}$ to $d\boldsymbol{\mathcal{L}}_m$ except at frequencies of the flexible modes of the top-plate. The Simscape model can therefore be used to develop the control strategies.

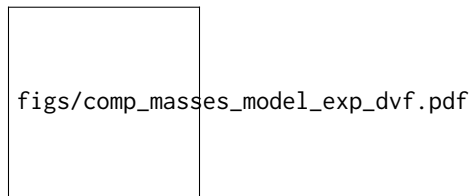## 4.2 Comparison with the Simscape model

Let's now compare the identified dynamics with the Simscape model. We wish to verify if the Simscape model is still accurate for all the tested payloads.

4.2.1 System Identification

Let's initialize the simscape model with the nano-hexapod fixed on top of the vibration table. First perform the identification for the transfer functions from $\boldsymbol{u}$ to $d\boldsymbol{\mathcal{L}}_m$: The identified dynamics are then saved for further use.

4.2.2 Transfer function from Actuators to Encoders

The measured FRF and the identified dynamics from u_i to $d\mathcal{L}_{m,i}$ are compared in Figure 4.8. A zoom near the "suspension" modes is shown in Figure 4.9.

figs/comp_masses_model_exp_dvf.pdf

Figure 4.8: Comparison of the transfer functions from u_i to $d\mathcal{L}_{m,i}$ - measured FRF and identification from the Simscape model

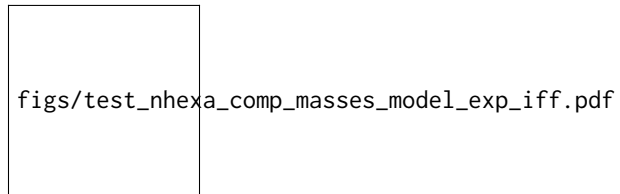figs/test_nhexa_comp_masses_model_exp_dvf_zoom.pdf
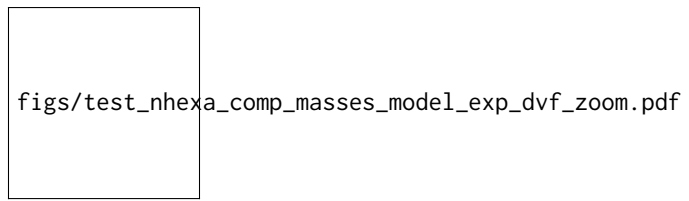
Figure 4.9: Comparison of the transfer functions from u_i to $d\mathcal{L}_{m,i}$ - measured FRF and identification from the Simscape model (Zoom)

> **Important**
>
> The Simscape model is very accurately representing the measured dynamics up. Only the flexible modes of the struts and of the top plate are not represented here as these elements are modelled as rigid bodies.

4.2.3 Transfer function from Actuators to Force Sensors

The measured FRF and the identified dynamics from u_i to $\tau_{m,i}$ are compared in Figure 4.10. A zoom near the "suspension" modes is shown in Figure 4.11.

Figure 4.10: Comparison of the transfer functions from u_i to $\tau_{m,i}$ - measured FRF and identification from the Simscape model
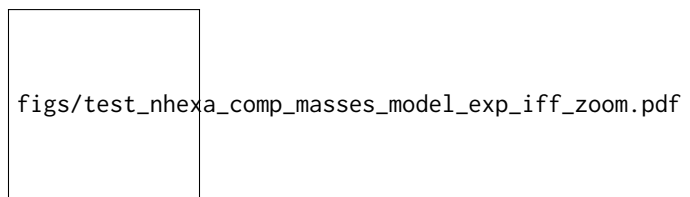
Figure 4.11: Comparison of the transfer functions from u_i to $\tau_{m,i}$ - measured FRF and identification from the Simscape model (Zoom)

Bibliography

[1] S. Skogestad and I. Postlethwaite, *Multivariable Feedback Control: Analysis and Design - Second Edition*. John Wiley, 2007.

[2] M. Indri and R. Oboe, *Mechatronics and Robotics: New Trends and Challenges*. CRC Press, 2020.